Photoanodes

DOI: 10.1002/anie.201406017

In Situ Preparation of a Ti^{3+} Self-Doped TiO_2 Film with Enhanced Activity as Photoanode by N_2H_4 Reduction**

Chengyu Mao, Fan Zuo, Yang Hou, Xianhui Bu, and Pingyun Feng**

Abstract: *A new synthetic method to fabricate Ti^{3+}-modified, highly stable TiO_2 photoanodes for H_2O oxidation is reported. With Ti foil as both the conducting substrate and the Ti^{3+}/Ti^{4+} source, one-dimensional blue Ti^{3+}/TiO_2 crystals were grown by a one-step hydrothermal reaction. The concentration of Ti^{3+} was further tuned by N_2H_4 reduction, leading to a greater photoelectrocatalytic activity, as evidenced by a high photocurrent density of 0.64 mA cm^{-2} at 1.0 V vs RHE under simulated AM 1.5 G illumination. Electron paramagnetic resonance and Mott–Schottky plots reveal that higher charge-carrier density owing to N_2H_4 reduction contributes to the observed improvement. The generality of this synthesis method was demonstrated by its effectiveness in improving the performance of other types of photoanodes. By integrating the advantages of the 1D TiO_2 architecture with those of Ti^{3+} self-doping, this work provides a versatile tool toward the fabrication of efficient TiO_2 photoanodes.*

Harvesting solar energy efficiently is critical for sustainable-energy supply and environmental conservation.[1] Artificial photosynthesis, which can convert solar energy directly into chemical energy, has been extensively investigated.[2] Since its first report in 1972,[3] TiO_2 has been considered as a promising photoanode[4] for water oxidation because of its photostability, non-toxicity, and abundance. However, its large band gap limits its activity to only UV radiation, a small portion of sunlight. Furthermore, short electron–hole recombination lifetime and the resulting carrier loss during charge transport greatly diminish its photo-to-current conversion efficiency. These drawbacks impede the performance of TiO_2 and its application as an efficient photoelectrocatalytic material.[5]

Recent studies aimed at improving the performance of catalytic materials have been focused on the architecture of nanostructured materials[6] and elemental doping.[7] One-dimensional nanostructured TiO_2 such as nanowires,[8] nanotubes,[9] and branched nanorods[10] can exhibit significant light absorption depth and short diffusion distance for charge carriers, facilitating light absorption and electron–hole separation simultaneously. Hwang et al. found that the photoelectrochemical (PEC) performance depends on the nanowire length and surfacing coating.[11] Shi et al. and Liu et al. reported the benefits of 3D nanowires and cross-linked nanowires on PEC performance.[12] Core–shell nanowires[13] were also reported as beneficial to water oxidation. In addition, foreign dopants such as C,[14] N,[15] F,[16] W,[17] and Sn[18] or Ti^{3+} self-doping[19] by hydrogenation,[20] electrochemical reactions[21] and chemical reductions[22] have been employed to extend the light absorption spectrum into visible range, and to enhance electronic conductivity as well as electron–hole separation efficiency. In some cases, the morphology and composition control can be achieved simultaneously, leading to enhanced water oxidation performance under sunlight illumination. Hoang et al. developed N-modified TiO_2 nanowires through nitridation in NH_3 flow.[25a] Wang et al.[23] and Cho et al.[24] synthesized TiO_2 nanowires with oxygen vacancies through hydrogenation and CO flame reduction, respectively. Hoang et al. also made TiO_2 nanowires with synergistic Ti^{3+} and N doping.[25b]

Photoanodes mentioned above are generally prepared on fragile fluorine-doped tin oxide (FTO) glasses and separate steps are often needed to obtain the desired morphology and doping level. Herein, we demonstrate a facile synthetic method for generating 1D crystalline rutile photoanode with simultaneous Ti^{3+} self-doping inside the sample. A subsequent hydrothermal treatment in N_2H_4 can further enhance its performance in water oxidation by increasing the Ti^{3+} concentration. We also show that this method can be applied to other well-developed TiO_2 materials, which makes our strategy versatile for improving the catalytic performance of TiO_2-based materials.

Rutile TiO_2 with Ti^{3+} self-doping was grown on a Ti foil substrate hydrothermally. In contrast to many previous reports requiring Ti^{IV} sources, such as Ti^{IV} alkoxide and $TiCl_4$, Ti foil plays a dual role in this case, as both substrate and Ti^{III}/Ti^{IV} source during the synthesis.[26] Unlike anodization and other synthesis strategies which involve electrochemical process or F-containing agents and would ultimately lead to anatase phase, Ti metal was dissolved in a dilute HCl aqueous solution and Ti^{III}/Ti^{IV} were formed spontaneously on the surface of the Ti substrate and subsequently formed oxide films, which then act as a protective layer to prohibit further dissolution of the Ti substrate.

[*] C. Mao, Prof. P. Feng
Materials Science and Engineering Program
University of California
Riverside, CA 92521 (USA)
E-mail: pingyun.feng@ucr.edu
Dr. F. Zuo, Dr. Y. Hou, Prof. P. Feng
Department of Chemistry, University of California
Riverside, CA 92521 (USA)
Prof. X. Bu
Department of Chemistry and Biochemistry, California State University, Long Beach, CA 90840 (USA)

[**] This work is supported by NSF CHE-1213795 (P.F.). The SEM was carried out at UCR Central Facility for Advanced Microscopy and Microanalysis (CFAMM). XPS is supported by NSF DMR-0958796.

Supporting information for this article is available on the WWW under http://dx.doi.org/10.1002/anie.201406017.

 © 2014 Wiley-VCH Verlag GmbH & Co. KGaA, Weinheim

The concentration of anions (Cl^-) plays a critical role in the synthesis. The doubling of [Cl^-] by adding NaCl without pH change can completely dissolve the substrate to give white powders whereas acids, such as HNO_3 and H_2SO_4, with the same [H^+] produced no product. The as-formed Ti^{IV} was partially reduced to give a Ti^{3+} self-doped TiO_2 film on the Ti substrate. Unlike FTO glass can easily break or lose conductivity under the harsh conditions, the Ti metal substrate is more stable and flexible for further treatment or device fabrication and maintains a good conductivity throughout these processes. The as-prepared sample was annealed in Ar to further increase the contact with the Ti substrate and to prevent possible loss of Ti^{3+} by oxidation in air. The resulting sample is denoted as R-TiO_2-F. Subsequent treatment with a strong reducing agent, N_2H_4, was conducted to generate TiO_2 (denoted as RR-TiO_2-F) films with a higher Ti^{3+} doping level (details in the Supporting Information).

Ti foil turned from silvery to blue after the hydrothermal reaction owing to the formation of a Ti^{3+}/TiO_2 layer on the surface. Powder X-ray diffraction (PXRD) confirms the formation of rutile TiO_2 (Figure S3a in the Supporting Information). The strong Ti peak shows that the majority of the Ti substrate is preserved after the hydrothermal reaction. High-magnification SEM images (Figure S4a) reveal that the rutile film grown on the substrate has in fact a 1D architecture with a pyramid-like end. The shape of the crystals grown on the substrate is similar to the previously synthesized bulk Ti^{3+}-doped TiO_2 with active facets.[27] Compared to most 1D photoanode TiO_2 materials, the photoanode films synthesized herein with clean surface and clear facets are unique and rare. The cross-sectional image (Figure S4c) shows the interface between the surface structure and substrate, confirming our proposed layout. It is expected that such an architecture could facilitate charge separation and efficient light adsorption compared to that of the bulk films and nanoparticles. From PXRD, no significant loss of crystallinity was observed for N_2H_4 treated samples RR-TiO_2-F (Figure S3a), indicating the high chemical stability of the as-prepared sample. Furthermore, no shape and morphology change upon treatment was observed according to SEM image (Figure 1 b).

X-ray photoemission spectroscopy (XPS) was used to study the surface composition of the TiO_2 film grown on the Ti substrate. Ti $2p_{3/2}$ and O 1s XPS peaks (Figure S2) confirmed the formation of TiO_2. However, there is no XPS evidence for Ti^{3+}. This is because Ti^{3+} in the sample was embedded within the bulk and XPS only probes the surface. In addition, Ti^{3+} is susceptible to oxidation by O_2 in air and cannot survive long on the surface. Electron paramagnetic resonance spectra (EPR) recorded at 100 K were used to verify the presence of Ti^{3+} in our sample. It is difficult to collect strong enough EPR signals from the film sample because only a thin layer was grown on the surface. Thus, powder samples were synthesized under exactly the same reaction conditions as those for the film except that the Ti foil was replaced by Ti powder to make enough sample for EPR data collection (denoted as R-TiO_2-P details in Supporting Information). PXRD and SEM images (Figure S3b, S4b) showed that the prepared powder samples have the same crystallinity and morphology as the sample on the Ti foil substrate. As shown in Figure 1 a, a prominent signal at $g = 1.97$ unambiguously demonstrates the presence of Ti^{3+} in the bulk. A weak signal at $g = 2.007$ may come from surface resonances[28] of the oxygen-centered surface hole trapping sites generated during the annealing process. An order of magnitude intensity improvement at $g = 1.97$ for N_2H_4 reduced R-TiO_2-P (denoted as RR-TiO_2-P, details in Supporting Information) demonstrates a much higher Ti^{3+} concentration after N_2H_4 treatment. The absence of signals at $g = 2.02$ further excludes the presence of surface Ti^{3+}.

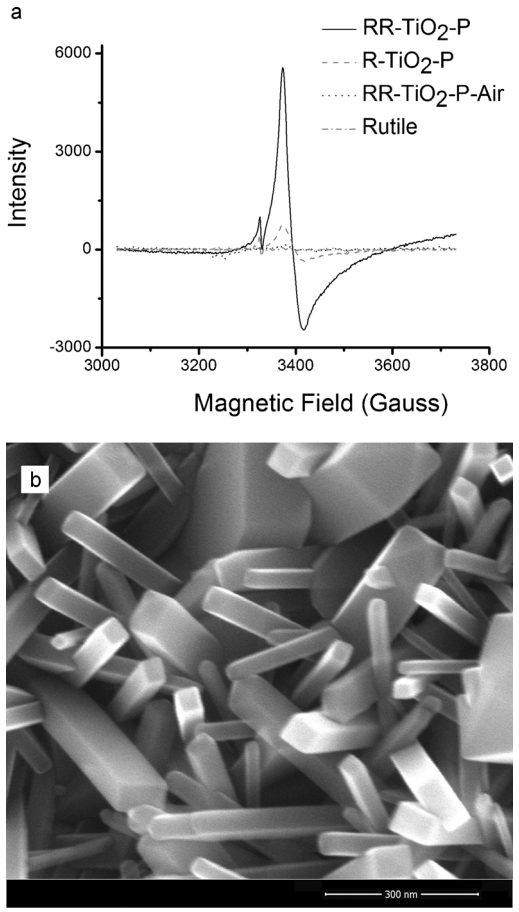

Figure 1. a) EPR spectra (100 K) for R-TiO_2-P, RR-TiO_2-P, RR-TiO_2-P-Air (RR-TiO_2-P heated in air, details in Supporting Information), and pristine rutile b) Typical SEM image of RR-TiO_2-F. Scale bar 300 nm.

To evaluate their water-oxidation performance as a photoanode, PEC measurements were conducted in a three-electrode electrochemical system, using 1M KOH aqueous solution as electrolyte and 100 mW cm^{-2} simulated sunlight illumination from a 150 W xenon lamp coupled with an AM 1.5G filter (details in Supporting Information).

Linear sweep voltammetry data from R-TiO_2-F and RR-TiO_2-F is shown in Figure 2 a. The onset potentials are almost the same (0.26 V and 0.23 V vs reversible hydrogen electrode (RHE), respectively (see Supporting Information for details of the conversion of values obtained vs Ag/AgCl into vs RHE), indicating a comparable surface kinetics. However, the photocurrent density almost doubled from 0.36 mA cm^{-2}

 © 2014 Wiley-VCH Verlag GmbH & Co. KGaA, Weinheim

to 0.69 mA cm^{-2} at 1.23 V vs RHE. Figure 2b shows the corresponding photoconversion efficiency η calculated by the equation: $\eta = J_{ph}(1.23 - V_{RHE})/P$, where P is the power density of illumination light and J_{ph} is the current density. The optimum efficiency comes where enough photocurrent is generated while the applied bias does not negate the advantage of shining light. RR-TiO_2-F exhibits a peak value of 0.36 % (0.49 V vs RHE), nearly tripling that of R-TiO_2-F, which is only 0.14 % (0.53 V vs RHE). Prompt and reproducible photoresponses upon illumination of both samples were revealed from the transient photocurrents measured at a fixed bias potential of 1.0 V vs RHE <. As shown in Figure 2c, the rise and fall of the photocurrent corresponded well to the switching on and off of irradiation. The current densities for R-TiO_2-F and RR-TiO_2-F are 0.35 mA cm^{-2} and 0.64 mA cm^{-2}, matching well with the results from linear sweep voltammetry. Photocurrent under visible light irradiation (over 400 nm, Figure S5b,S5c) was also measured for both samples. RR-TiO_2-F shows a better photoresponse than that of R-TiO_2-F, though the photocurrent itself only experienced a 46 % increase, from 36 μA cm^{-2} to 53 μA cm^{-2}.

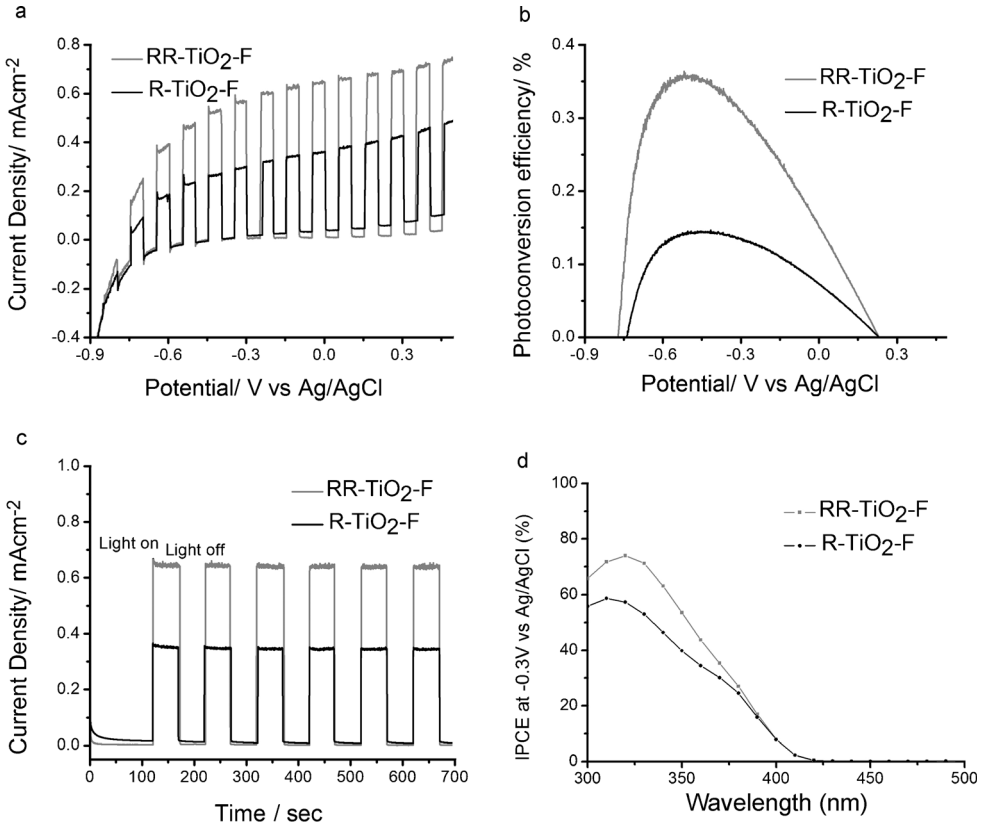

Figure 2. a) Linear sweep voltammetry (scan rate of 10 mV s^{-1}) with chopped light; b) Photoconversion efficiency; c) Transient photocurrent density over time; and d) IPCE for R-TiO_2-F and RR-TiO_2-F.

To better understand their performance, the incident photon-to-current conversion efficiencies (IPCE)[29] were measured at 0.7 V versus RHE (details in Supporting Information). IPCE allows the study of materials' PEC performance as a function of incident beam wavelength and excludes the effects of different light sources and filters. For example, the photocurrent for RR-TiO_2-F obtained by integrating IPCE multiplied by AM 1.5 G energy flux over the range of 300–500 nm is 0.61 mA cm^{-2}. The discrepancy between the measurement under AM 1.5 G irradiation at the same bias (0.58 mA cm^{-2}) and the integration method might come from the difference between the simulated light and standard AM 1.5 G. IPCE is determined by three key factors involved in PEC, as shown in Equation (1)

$$\mathrm{IPCE}(\lambda) = \eta_{e^-/h^+}(\lambda)\,\eta_{transport}(\lambda)\,\eta_{transfer}(\lambda) \quad (1)$$

where $\eta_{e^-/h^+}(\lambda)$, $\eta_{transport}(\lambda)$ and $\eta_{transfer}(\lambda)$ represent the efficiencies for photon absorbance, charge transport within the electrode, and charge transfer at the electrode/electrolyte interface, respectively.[30] As shown in the UV/Vis spectrum obtained by their corresponding reflectance spectra (Figure S6b), R-TiO_2-F and RR-TiO_2-F have comparable light adsorption. The minor difference here cannot account for a big difference in the activity. From Figure 2d we note both samples have an adsorption edge around 420 nm. RR-TiO_2-F begins to triumph when the wavelength is shorter than 370 nm, allowing this portion of light to make a major contribution to the photocurrent enhancement. Given that higher energy photons are mainly adsorbed near the tip of 1D TiO_2 and electrons generated there need to travel a longer distance to reach the current collector, an enhanced electron mobility should be achieved in RR-TiO_2-F to facilitate this charge transport, namely a more efficient $\eta_{transport}(\lambda)$.

To validate our postulate that improved electron conductivity contributes to a better performance, we compared electrochemical impedance spectra (EIS) of R-TiO_2-F and RR-TiO_2-F in dark and illumination conditions. The radius of the arcs of Nyquist plots shown in Figure 3a is associated directly with the charge-transfer process and a smaller radius is correlated with a more efficient charge transfer. For both samples, a much smaller arc was obtained under illumination, suggesting less charge-transfer resistance. Significantly, RR-TiO_2-F showed an arc more compressed than that of R-TiO_2-F both in dark and under irradiation, suggesting a better charge-transfer process

 © 2014 Wiley-VCH Verlag GmbH & Co. KGaA, Weinheim

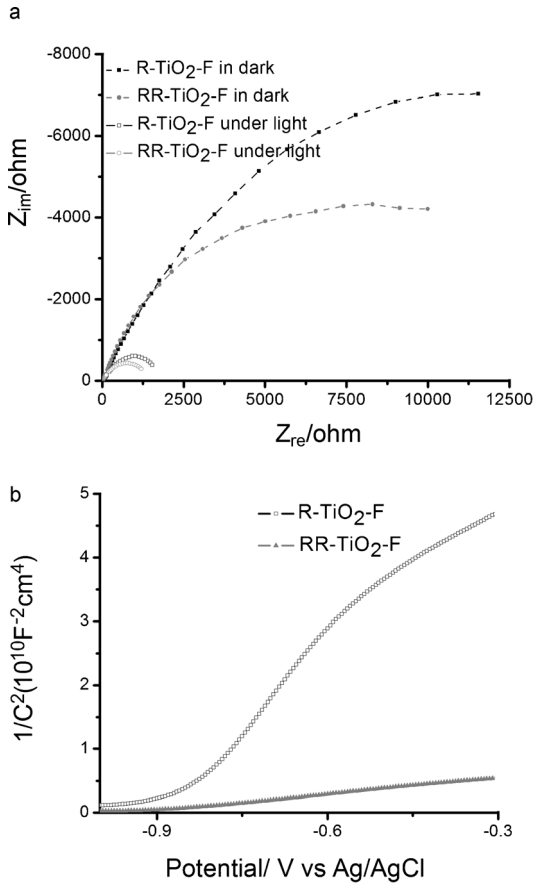

Figure 3. a) Nyquist plots for R-TiO_2-F and RR-TiO_2-F in the dark and under illumination. b) Mott–Schottky plots for R-TiO_2-F and RR-TiO_2-F in the dark.

and thus a more effective separation of photo-generated electron–hole pairs.

To gain further insight into the charge-transfer process and the impact of N_2H_4 reduction on the electronic structures, Mott–Schottky plots were collected at 5 kHz in the dark (Figure 3b). A positive slope in the plot is a direct evidence of n-type semiconductor, as expected from TiO_2 photoanode. Moreover, a substantially shallower slope for RR-TiO_2-F with higher Ti^{3+} concentration was obtained compared to R-TiO_2-F, suggesting an increase of donor density after N_2H_4 reduction. Carrier density of each sample can be calculated from the corresponding slope using Equation (2).

$$N_d = \frac{2/e_0\varepsilon\varepsilon_0}{d(1/C^2)/dV} \quad (2)$$

We take $\varepsilon = 170$ for rutile TiO_2[31] and the calculated electron densities of R-TiO_2-F and RR-TiO_2-F were 6.9×10^{18} cm^{-3} and 8.54×10^{19} cm^{-3}, respectively. Though the absolute value of donor density calculated from a flat-electrode model may not be accurate, a dramatic enhancement of donor density is unambiguously supported by a qualitative comparison of the slopes, considering the intact morphology and phase upon reduction. This increase in charge-carrier density gives rise to improved electronic conductivity and thus a better electron–hole pair separation and transport ($\eta_{transport}(\lambda)$) within the electrode. Moreover, The upward shift of Fermi level[32] caused by higher donor density could further facilitate the charge-transfer kinetics at the electrode/electrolyte interface, which is another fundamental factor affecting IPCE in addition to charge transport within the bulk materials. On the contrary, a depressed donor density would impair the charge separation and thus lower the PEC performance. Upon being heated in air for only 1 h, R-TiO_2-F lost most of its activity and the photocurrent became lower than 0.1 mA cm^{-2}. The donor density decreased to 5.7×10^{16} cm^{-3} and an enlarged arc appeared in Nyquist plot, as shown in Figure S7. The lack of a signal for Ti^{3+} in the corresponding powder sample's EPR spectrum is also consistent with its lowered Ti^{3+} level.

To verify that this facile N_2H_4 reduction is a general strategy for enhancing the water-oxidation performance of the TiO_2 photoanode, we also conducted similar experiments for TiO_2 nanowires grown on FTO (denoted as TiO_2-FTO).

The pristine nanowire on FTO was prepared by a reported method.[11] Both XRD and SEM characterizations (Figure S8,S10) confirmed the formation of nanowires on FTO. The photocurrent density obtained from PEC measurement (0.71 mA cm^{-2} at 1.0 V vs RHE) was also comparable with previous reports. While no morphology or phase change was observed after the reduction, photocurrent density underwent a nearly 1-fold increase to 1.32 mA cm^{-2} at the same bias (Figure 4a). Given the fact that 1.8 mA cm^{-2} is thermodynamically maximum achievable photocurrent of rutile under AM 1.5 G illumination by adsorbing all incoming photons with energies above its band gap, N_2H_4 reduced TiO_2-FTO (denoted as R-TiO_2-FTO) utilized 73% available photons and is among the best of TiO_2 photoanodes under AM 1.5 G illumination. Even under visible light illumination (>400 nm), R-TiO_2-FTO can still keep 18% (0.24 mA cm^{-2}) of its total current, tripling that of the pristine one (Figure 4b). IPCE measurement again confirmed the enhanced photocurrent is due to an elevated utilization of UV portion, especially those with a wavelength shorter than 380 nm (Figure 4c).

In summary, we have developed a novel method to grow one-dimensional crystalline rutile TiO_2 directly on a flexible Ti metal substrate for the first time. Self-doping by Ti^{3+} is also realized in the same step. We also demonstrate the N_2H_4 reduction as a facile and general method that provides a higher Ti^{3+} self-doping level and greatly improves water-oxidation performance for TiO_2 materials. The boost in photocurrent shown herein should result from an enhanced donor density and thus higher electronic conductivity brought about by the reduction process, as confirmed by EPR spectra and impedance analysis. The newly developed Ti metal/TiO_2 layout creates new opportunities for device fabrication in various related fields and allows treatment of TiO_2 even under harsh conditions without damaging the substrate. This simple but effective reduction method also provides a general and promising route for enhancing the properties of a large number of existing semiconductors.

 © 2014 Wiley-VCH Verlag GmbH & Co. KGaA, Weinheim

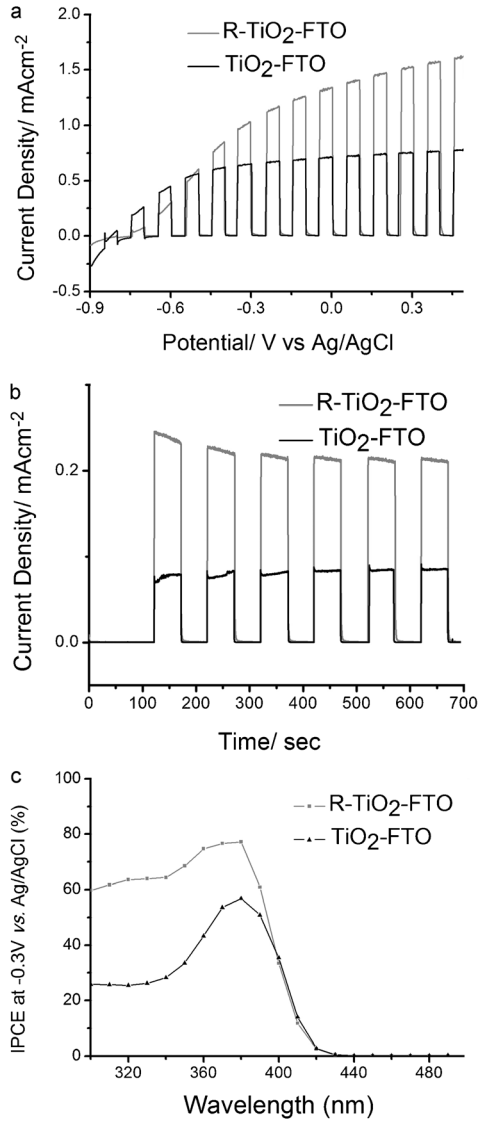

Figure 4. a) Linear sweep voltammetry with chopped light; b) transient photocurrent density over time under visible light; and c) IPCE for TiO_2-FTO and R-TiO_2.

Received: June 8, 2014
Published online: August 1, 2014

Keywords: photoanodes · self-doped TiO_2 · titanium · water oxidation

[1] N. S. Lewis, *Science* **2007**, *315*, 798 – 801.
[2] a) S. Fu, Y. Liu, Y. Ding, X. Du, F. Song, R. Xiang, B. Ma, *Chem. Commun.* **2014**, *50*, 2167 – 2169; b) J. Gao, J. Miao, P.-Z. Li, W. Y. Teng, L. Yang, Y. Zhao, B. Liu, Q. Zhang, *Chem. Commun.* **2014**, *50*, 3786 – 3788.
[3] A. Fujishima, K. Honda, *Nature* **1972**, *238*, 37 – 38.
[4] S. U. M. Khan, M. Al-Shahry, W. B. Ingler, *Science* **2002**, *297*, 2243 – 2245.
[5] X. Chen, S. Shen, L. Guo, S. S. Mao, *Chem. Rev.* **2010**, *110*, 6503 – 6570.
[6] a) Y.-C. Pu, G. Wang, K.-D. Chang, Y. Ling, Y.-K. Lin, B. C. Fitzmorris, C.-M. Liu, X. Lu, Y. Tong, J. Z. Zhang, Y.-J. Hsu, Y. Li, *Nano Lett.* **2013**, *13*, 3817 – 3823; b) L. Fuoco, U. A. Joshi, P. A. Maggard, *J. Phys. Chem. C* **2012**, *116*, 10490 – 10497; c) Y. Xu, R. Xu, J. Cui, Y. Liu, B. Zhang, *Chem. Commun.* **2012**, *48*, 3881 – 3883.
[7] a) Y. Tan, C. Xu, G. Chen, X. Fang, N. Zheng, Q. Xie, *Adv. Funct. Mater.* **2012**, *22*, 4584 – 4591; b) Y. Ling, G. Wang, D. A. Wheeler, J. Z. Zhang, Y. Li, *Nano. Lett.* **2011**, *11*, 2119 – 2125; c) H. Tantang, J. Xiao, J. Wei, M. B. E. Chan-Park, L.-J. Li, Q. Zhang, *Eur. J. Inorg. Chem.* **2011**, 4182 – 4186.
[8] a) B. Liu, E. S. Aydil, *J. Am. Chem. Soc.* **2009**, *131*, 3985 – 3990; b) X. Feng, K. Shankar, O. K. Varghese, M. Paulose, T. J. Latempa, C. A. Grimes, *Nano. Lett.* **2008**, *8*, 3781 – 3786; c) B. Tan, Y. Wu, *J. Phys. Chem. B* **2006**, *110*, 15932 – 15938.
[9] a) P. Roy, S. Berger, P. Schmuki, *Angew. Chem.* **2011**, *123*, 2956 – 2995; *Angew. Chem. Int. Ed.* **2011**, *50*, 2904 – 2939; b) A. Wolcott, W. A. Smith, T. R. Kuykendall, Y. Zhao, J. Z. Zhang, *Small* **2009**, *5*, 104 – 111; c) Z. Zhang, P. Wang, *Energy Environ. Sci.* **2012**, *5*, 6506 – 6512.
[10] I. S. Cho, Z. Chen, A. J. Forman, D. R. Kim, P. M. Rao, T. F. Jaramillo, X. Zheng, *Nano. Lett.* **2011**, *11*, 4978 – 4984.
[11] Y. J. Hwang, C. Hahn, B. Liu, P. Yang, *ACS Nano* **2012**, *6*, 5060 – 5069.
[12] a) M. Liu, N. de Leon Snapp, H. Park, *Chem. Sci.* **2011**, *2*, 80 – 87; b) J. Shi, Y. Hara, C. Sun, M. A. Anderson, X. Wang, *Nano. Lett.* **2011**, *11*, 3413 – 3419.
[13] Y. J. Hwang, A. Boukai, P. Yang, *Nano Lett.* **2008**, *9*, 410 – 415.
[14] J. H. Park, S. Kim, A. J. Bard, *Nano Lett.* **2005**, *6*, 24 – 28.
[15] R. Asahi, T. Morikawa, T. Ohwaki, K. Aoki, Y. Taga, *Science* **2001**, *293*, 269 – 271.
[16] G. Wu, J. Wang, D. F. Thomas, A. Chen, *Langmuir* **2008**, *24*, 3503 – 3509.
[17] I. S. Cho, C. H. Lee, Y. Feng, M. Logar, P. M. Rao, L. Cai, D. R. Kim, R. Sinclair, X. Zheng, *Nat. Commun.* **2013**, *4*, 1723.
[18] M. Xu, P. Da, H. Wu, D. Zhao, G. Zheng, *Nano Lett.* **2012**, *12*, 1503 – 1508.
[19] F. Zuo, L. Wang, T. Wu, Z. Zhang, D. Borchardt, P. Feng, *J. Am. Chem. Soc.* **2010**, *132*, 11856 – 11857.
[20] X. Chen, L. Liu, P. Y. Yu, S. S. Mao, *Science* **2011**, *331*, 746 – 750.
[21] Z. Zhang, M. N. Hedhili, H. Zhu, P. Wang, *Phys. Chem. Chem. Phys.* **2013**, *15*, 15637 – 15644.
[22] a) Q. Kang, J. Cao, Y. Zhang, L. Liu, H. Xu, J. Ye, *J. Mater. Chem. A* **2013**, *1*, 5766 – 5774; b) B. H. Meekins, P. V. Kamat, *ACS Nano* **2009**, *3*, 3437 – 3446; c) Z. Zheng, B. Huang, X. Meng, J. Wang, S. Wang, Z. Lou, Z. Wang, X. Qin, X. Zhang, Y. Dai, *Chem. Commun.* **2013**, *49*, 868 – 870.
[23] G. Wang, H. Wang, Y. Ling, Y. Tang, X. Yang, R. C. Fitzmorris, C. Wang, J. Z. Zhang, Y. Li, *Nano Lett.* **2011**, *11*, 3026 – 3033.
[24] I. S. Cho, M. Logar, C. H. Lee, L. Cai, F. B. Prinz, X. Zheng, *Nano Lett.* **2013**, *14*, 24 – 31.
[25] a) S. Hoang, S. Guo, N. T. Hahn, A. J. Bard, C. B. Mullins, *Nano Lett.* **2012**, *12*, 26 – 32; b) S. Hoang, S. P. Berglund, N. T. Hahn, A. J. Bard, C. B. Mullins, *J. Am. Chem. Soc.* **2012**, *134*, 3659 – 3662.
[26] H. Zhang, Y. Wang, P. Liu, Y. Han, X. Yao, J. Zou, H. Cheng, H. Zhao, *ACS Appl. Mater. Interfaces* **2011**, *3*, 2472 – 2478.
[27] F. Zuo, K. Bozhilov, R. J. Dillon, L. Wang, P. Smith, X. Zhao, C. Bardeen, P. Feng, *Angew. Chem.* **2012**, *124*, 6327 – 6330; *Angew. Chem. Int. Ed.* **2012**, *51*, 6223 – 6226.
[28] D. C. Hurum, A. G. Agrios, K. A. Gray, T. Rajh, M. C. Thurnauer, *J. Phys. Chem. B* **2003**, *107*, 4545 – 4549.
[29] T. Bak, J. Nowotny, M. Rekas, C. C. Sorrell, *Int. J. Hydrogen Energy* **2002**, *27*, 991 – 1022.
[30] Z. Chen, T. F. Jaramillo, T. G. Deutsch, A. Kleiman-Shwarsctein, A. J. Forman, N. Gaillard, R. Garland, K. Takanabe, C. Heske, M. Sunkara, E. W. McFarland, K. Domen, E. L. Miller, J. A. Turner, H. N. Dinh, *J. Mater. Res.* **2010**, *25*, 3 – 16.
[31] R. A. Parker, *Phys. Rev.* **1961**, *124*, 1719 – 1722.
[32] D. C. Cronemeyer, *Phys. Rev.* **1959**, *113*, 1222 – 1226.

 © 2014 Wiley-VCH Verlag GmbH & Co. KGaA, Weinheim